Green One-Step Synthesis of Medical Nanoagents for Advanced Radiation Therapy

Daniela Salado Leza, Erika Porcel, Xiaomin Yang, Lenka Stefancikova, Marta Bolsa-Ferruz, Farah Savina, Diana Dragoe, Jean-Luc Guerquin-Kern, Ting-Di Wu, Ryoichi Hirayama, et al.

RESEARCH ARTICLE

Green one-step synthesis of medical nanoagents for advanced radiation therapy

Daniela Salado-Leza,[a] [b] Erika Porcel,[a] Xiaomin Yang,[a] Lenka Štefančíková,[a] Marta Bolsa-Ferruz,[a] Farah Savina,[a] Diana Dragoe,[c] Jean-Luc Guerquin-Kern,[d] Ting-di Wu,[d] Ryoichi Hirayama,[e] Hynd Remita,[f] and Sandrine Lacombe*[a]

[a] Dr. D. Salado-Leza, Dr. E. Porcel, M.Sc. X. Yang, Dr. L. Štefančíková, Dr. M. Bolsa-Ferruz, F. Savina, Prof. Dr. S. Lacombe
Institut des Sciences Moléculaires d'Orsay (UMR 8214) CNRS, Université Paris-Saclay, 91405 Orsay, France
E-mail: sandrine.lacombe@u-psud.fr
[b] Dr. D. Salado-Leza
Cátedras CONACyT, Universidad Autónoma de San Luis Potosí, Facultad de Ciencias Químicas, Av. Dr. Manuel Nava 6, Zona Universitaria, 78210 San Luis Potosí, S.L.P., Mexico
[c] Dr. D. Dragoe
Institut de Chimie Moléculaire et des Matériaux d'Orsay (UMR 8182) CNRS, Université Paris-Saclay, 91405 Orsay, France
[d] Dr. J-L. Guerquin-Kern, Dr. T. Wu
Laboratoire d'Imagerie Integrative, Institut Curie, INSERM (U759), Université Paris Sud, building 112, 91405 Orsay Cedex, France
[e] Dr. R. Hirayama
Department of Charged Particle Therapy Research, National Institute of Radiological Sciences, National Institutes for Quantum and Radiological Science and Technology, Chiba, 263-8555, Japan
[f] Dr. H. Remita
Institut de Chimie Physique (UMR 8000) CNRS, Université Paris Saclay, 91405 Orsay Cedex, France

Supporting information for this article is given via a link at the end of the document.

Abstract: Metal-based nanoparticles (NPs) have attracted great attention to amplify and improve the tumour targeting of medical radiations. However, their fast, simple and reproducible production remains a challenge. Currently, NPs are synthesized by chemical methods or radiolysis using toxic reactants. The waste of time, loss of material and potential environmental hazards are major limitations. This work proposes a simple, fast and green strategy to synthesize small, non-toxic and stable NPs in water with a 100% production rate. Radiolysis is used to simultaneously synthesize and sterilize NPs solutions. The synthesis of platinum nanoparticles (PtNPs) coated with biocompatible ligands is presented as proof of concept. PtNPs have the singular property of amplifying the cell killing induced by γ-rays (18%) and even more the effects of carbon ions (44%) used in hadrontherapy. They induce nanosize molecular damage, a major finding to potentially implement this protocol in treatment planning simulations. Hence, the new eco-friendly, fast and simple method proposed opens a new era of engineering NPs and boosts the development of NPs-aided radiation therapies.

Introduction

The addition of metallic compounds was proposed two decades ago as a novel strategy to enhance the biological efficiency of medical radiations. [1] Biston and co-workers showed the efficiency of combining cisplatin, a commonly used platinum antineoplastic drug, with conventional radiotherapy to improve gliomas treatment. [2] To selectively increase the toxic effects of radiation, agents capable of concentrating in the tumour have been introduced such as small nanoparticles. Hainfeld and co-workers demonstrated that glucose coated gold NPs extend the life of mice treated with 160 kV X-rays. [3,4] Moreover, Yan Li and co-workers proved that porous platinum nanoparticles (Pt NPs) enhance conventional radiation therapy using 250 kV X-rays.[5] Currently, clinical trials are in progress to evaluate the efficiency of hafnium oxide (NBTXR3 - Nanobiotix (Paris, France)) [6], gadolinium based (AGuIX- NH-TherAguix (Grenoble, France)), [7,8] and gold (CYT-6091 CytImmune -USA)) [9] nanoagents as radio-enhancing or antineoplastic compounds.

Previous experiments have demonstrated that the enhancing effect of high-Z nanoparticles is due to the induction of nanosize damage triggered by the production of electron bursts and radical clusters in the vicinity of the agent, far from the nucleus. [10–12] More interestingly, the use of metallic nanoparticles was found to be effective not only in the case of conventional radiation treatments (using X-rays or γ-rays), but also with ion beams, a modality that is superior to conventional radiotherapy. Shortly, hadrontherapy is based on the use of charged particles (protons or carbon ions) accelerated to high energies (70 to 400 MeV/a.m.u.) to eradicate the intractable radio-resistant tumours. [13,14] Compared to conventional radiotherapy, it presents two main advantages: a precise ballistic effect with a finite range and a maximum dose deposition at the end of the ion tracks (Bragg peak) which prevents damage in the surrounding healthy tissue, and a relative biological efficiency of carbon ions that is two to four times superior to the effect of electromagnetic radiations (X and gamma rays) which prevents any resistance to the treatment. [15] In this context, Kaur and co-workers showed that the addition of glucose capped gold nanoparticles improve the treatment of HeLa cells by 62 MeV carbon ions. [16] Kim and co-workers demonstrated that the effect of 40 MeV protons is enhanced in the presence of gold and iron oxide nanoparticles using a CT26 mouse model. [17]. Even if the physicochemical mechanism proposed in this work was controversial, [18,19] the work evidenced, for the first time, the radio-enhancement of proton treatment using

metallic nanoparticles. Recently, antibody-functionalized gold nanoparticles and other high-Z containing nanoparticles (*e.g.* Gd_2O_3 NCs, Fe_2O_3 NPs, Pt NDs and Bi NRs) were tested, using colon, lung and breast cancer cell models treated by protons (2 MeV and 150 MeV) and carbon ions (100 MeV/a.m.u, LET= 50 keV/μm). [20–22] Our group demonstrated that mono- and bimetallic gold, platinum as well as gadolinium based nanoagents increase the induction of complex biodamage when photons (^{60}Co γ-rays) [23], proton (150 MeV) [24] or medical carbon beams (276 MeV/a.m.u) are used as ionizing radiations. [25] We also demonstrated that gadolinium based nanoparticles amplify the cell killing induced by ion beams. [26]

Considering the tremendous potential of metallic NPs to improve the performances of conventional and ion beam radiation therapies, the production of ready-to-use colloidal solutions is a critical challenge. Radio-enhancing nanoagents composed of gold, [27] hafnium, [28] gadolinium [29] and also platinum, [30] are commonly produced *via* chemical procedures. The use of chemicals that are often toxic and non-biodegradable, may present environmental hazards and limits the production of nanoagents. In addition, these chemicals may contaminate the nanoparticles surface and contribute to their cytotoxicity. Hence, multiple separation-purification steps including adsorption of toxic chemicals, removal of pathogens and transformation of toxic into non-toxic form, are required to produce biocompatible, non-toxic and stable agents ready-to-use in clinic. These procedures are time consuming and result in an intrinsic loss of material.

Radiolysis is an alternative method to produce metallic nanoparticles of controlled size and shape in solution or on supports. Solvated electrons and hydrogen radicals produced by solvent radiolysis are strong reducing species. This method presents some major benefits: limited use of chemical reductants, high production yields of metallic compounds under mild conditions (temperature and pressure) and size monodispersity of nanoparticles. [31] Different types of metallic nanoparticles have been synthesized following this methodology (see Table 1). However, in the studies currently existing, stabilizers and organic solvents potentially toxic and presenting environmental hazards were used and the final products are not adapted to medical use. Therefore, the development of efficient protocols able to produce non-toxic metallic nanoagents remains a challenge.

Table 1. Overview of high-Z based nanoparticles synthetized by radiolysis and their applications.

High-Z element	Size (nm)	Radiation	Chemicals	Research / Application	Ref
Au	57 to 120	X-rays,15.6 Gy.min^{-1}	Cetyltrimethylammonium bromide (CTAB) and L-ascorbic acid	Modelling of Au NPs formation	[32]
Au	2 to 22	γ-rays (^{60}Co), 1.5 Gy.s^{-1}	Leaf of *C. murale*	Biosynthesis assisted by radiation	[33]
Au	Aspect ratio= 3	γ-rays (^{60}Co), 3.4 kGy.h^{-1}	CTAB, isopropanol (IPA), acetone and Ag^+	Seedless synthesis of gold nanorods	[34]
Pt	~ 1.5	γ-rays (^{60}Co), 1.25 kGy.h^{-1}	Chitosan (CTS) and lactic acid	Synthesis and characterization	[35]
Pt	~ 7.4	γ-rays (^{60}Co), 600 Gy.min^{-1}	Sodium dodecyl sulfate (SDS) and IPA	Synthesis using SDS as capping agent	[36]
Pt	< 2.5	γ-rays (^{60}Co), 5 kGy.h^{-1}	Polyacrylic acid (PAA) and IPA	Oligomer clusters preparation	[37]
Pt	~ 3	γ-rays (^{60}Co), 2.2 kGy.h^{-1}	PAA	Improving radiation therapies	[25]
Pt	3 and 4.4	γ-rays (^{60}Co) -	Polyvinyl pyrrolidone (PVP), IPA, tetrahydrofuran (THF)	Size-controlled and optical properties	[38]
Pt	10 to 20	γ-rays (^{60}Co), 20 Gy.min^{-1}	Gelatin BDH and methanol	Catalytic activity tested by hydrogenation of C_2H_4	[39]
Gd	15 to 250	γ-rays (^{60}Co), 7.7 kGy h^{-1}	Chitosan and acetic acid	Synthesis for biomedical application	[40]

In this work, we developed a simple one-pot radiolysis-driven method to synthesize with a 100% production rate, biocompatible metallic nanoparticles dispersed in a sterile water solution, ready to use in clinic. In this work, the production of small platinum nanoparticles (Pt NPs) coated with poly (ethylene glycol) (PEG), a non-toxic polymeric coating approved by the FDA and the EU for internal consumption, is presented. The efficiency of these nanoagents to improve the effects of medical radiation beams was demonstrated and quantified on HeLa cells treated by γ-rays and medical carbon ions. To elucidate the molecular scale mechanisms induced by nanoparticles, experiments were performed using plasmids as bio-nanoprobes. This new green, rapid, reproducible and efficient method to produce stable and ready-to-use colloidal solutions of metallic nanoagents was recently registered for a patent.

Results and Discussion

An aqueous solution containing tetraammine platinum (II) chloride ($Pt(NH_3)_4Cl_2.H_2O$) and polyethylene glycol (PEG) ($H(OCH_2CH_2)_nOH$, M_W = 1000 g.mol^{-1}) with a PEG:Pt molar ratio of *ca.* 100, was de-aerated and then exposed to ^{60}Co gamma radiation (See Experimental Procedures at the Supporting Information). A colloid with a concentration in platinum of 10^{-2} mol.L^{-1} was obtained by applying a radiation dose of ~ 10 kGy. The mechanisms underpinning the formation of PtPEG NPs are

the following. [41–43] The excitation and ionization of water molecules by high energy radiation (γ-rays, X-rays, electrons or ion beams) leads to the production of radiolytic species (Equation 1). These species are homogeneously distributed in the bulk.

$$H_2O \xrightarrow{\gamma-rays} e_{aq}^-,\ H_3O^+,\ H^{\cdot},\ OH^{\cdot},\ H_2,\ H_2O_2 \quad (1)$$

The solvated electrons e_{aq}^- and hydrogen atoms $H^{\cdot}$ are strong reducing agents ($E^{\circ}(H_2O / e_{aq}^-) = -2.87\,V$ and $E^{\circ}(H^+ / H^{\cdot}) = -2.31\,V$). They efficiently reduce dissolved metal ions (M^{n+}) (Equations 2 and 3).

$$e_{aq}^- + M^{n+} \rightarrow M^{(n-1)+} \quad (2)$$

$$H^{\cdot} + M^{n+} \rightarrow H^+ + M^{(n-1)+} \quad (3)$$

Thus, the Pt^{II} precursor was reduced to the zero-valent state following the multi-step reaction: $Pt^{II} \rightarrow Pt^{I}$ and $Pt^{I} \rightarrow Pt^0$. The uniform energy deposited in the medium led to a homogeneous distribution of nucleation sites in the solution and the formation of metal clusters during the coalescence step with a remarkable monodispersity (Equation 4).

$$Pt^0 \rightarrow Pt_x^0 \rightarrow Pt_{x+1}^0 \quad (4)$$

PEG was used to limit the nucleation and growth steps, and increase the NPs stability in suspensions (Equation 4). The coating of the surface with PEG chains was achieved *in situ*, a remarkable advantage of our method.

The UV-vis absorption spectra showed that before irradiation the aqueous solution containing tetraammine platinum (II) chloride and PEG displayed an absorption peak at 240 nm and a small shoulder around 290 nm, which correspond to the ligand-to-metal charge transfer (LMCT) band of the precursor [44] (Figure S1). After irradiation, the appearance of a stretched absorption spectrum with a single broad peak centred at 270 nm, indicated the formation of small Pt aggregates. [42,44] The colour of the solution changed from colourless before irradiation to dark brown after irradiation (inset in Figure S1). The spectrum and the colour remained unchanged for several weeks indicating the complete reduction of the Pt^{II} precursor and the formation of stable PtPEG NPs.

High resolution-transmission electron microscopy (HR-TEM) (Figures 1a - c) revealed that PtPEG NPs were homogeneously formed as small spherical particles with an average core diameter of 3.2 ± 0.8 nm (Figure 1d). It corresponds to the assembly of *ca.* 1000 Pt atoms.

Dynamic Light Scattering (DLS) measurements (Figure 1e) of the as-synthesised PtPEG NPs showed an average hydrodynamic diameter of 8.8 ± 3.1 nm and a highly homogenous distribution. The surface charge (ζ-potential) was found close to -16.6 ± 5.1 mV in pure water (pH 6.2). The PZC or isoelectric point was observed at pH = 3, a result that reflects the good stability of the PtPEG NPs at the pH of the intracellular fluids (between 6.8 and 7.4). The negative ζ-potential is attributed to the –OH functional end-group of the PEG coating, which favours steric repulsion between particles preventing their aggregation. In addition, the observed negative charge suggests that PEG molecules thereby remain grafted at all pH values. This size and grafting is compatible with passive accumulation of NPs in tumours by the enhanced permeability and retention (EPR) effect. [45]

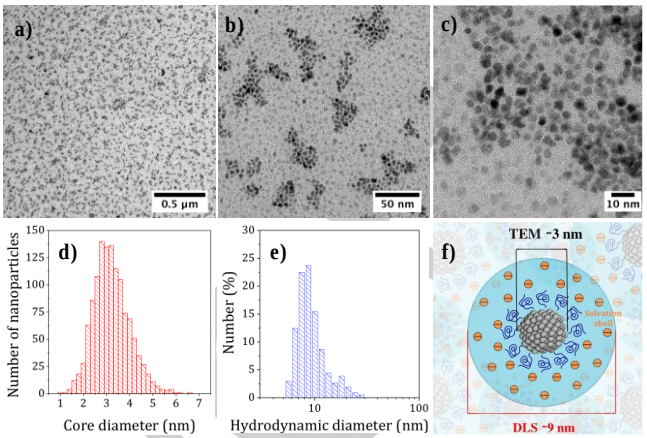

Figure 1. HR-TEM images of PtPEG NPs synthesized in water with an initial Pt^{II} concentration of 10^{-2} mol.L^{-1} and a PEG:Pt molar ratio of *ca.* 100, measured at different magnifications. Scale bars: (a) 0.5 µm, (b) 50 nm and (c) 10 nm. Size distribution of PtPEG NPs determined by (d) HR-TEM and (e) DLS. (e) Scheme of PtPEG NPs in aqueous solution.

The freshly prepared PEGylated NPs were stable in solution for a couple of months at 4°C. To optimize the long-term storage, they were successfully lyophilized using a two-step freeze-drying method. The lyophilized NPs were stored for several months at room temperature and re-suspension in various biocompatible buffers did not modify their characteristics.

X-ray photoelectron spectroscopy (XPS) was used to probe the result of the *in situ* PEGylation and verify the reduction of Pt^{II} into Pt^0. The survey XPS spectrum (not presented here – see Figure S2) revealed the presence of Pt, C, O, N and Cl, which confirmed the purity and elemental composition of the NPs. For a better clarity, narrow windows on the energy range of each element are presented in Figure 2.

Figure 2a displays the two spin-orbit components of Pt, [46,47] Pt-$4f_{7/2}$ and Pt-$4f_{5/2}$. The peaks were deconvoluted using Shirley background, symmetrical 70%-30% mixed Gaussian-Lorentzian shapes and a Doniach-Sunjic type function for the fit of metallic Pt peaks. The peaks at 71.2 and 74.4 eV correspond to zero-valent Pt atoms located at the NPs' bulk. The peaks at 70.4 and 73.7 eV correspond to Pt atoms located at the surface. This measurement confirms the complete reduction of Pt^{II} into Pt^0. Interestingly, the full width at half maximum (FWHM) of the peaks increased by about 33% (FWHM = 1.2 to 1.6 eV) in comparison ~~with~~ to the peaks of solid Pt. It indicates a strong interaction between the metallic surface and the PEG polymer. [48] The peak centered at 286.0 eV (Figure 2b) is characteristic of carbon adjacent to oxygen in an ether environment ~~(CH_2-O)~~ (C-O-C) and the small shoulder at a lower binding energy corresponds to the carbon-carbon bond in PEG. [49,50] The peak at 532.3 eV (Figure 2c) corresponds to the C-O-C (ether) and C-O-H (hydroxyl) oxygen. [49] The position and FWHM of the peaks remained unchanged, which is indicative of the formation of a PEG monolayer [50,51] perpendicular to the NP surface. [52] An overlap~~ping~~ between the peaks characteristic of aminated carbons (C-N, ~~-C-CN~~) at 286.0 ± 0.5 eV [53,54] and ~~double-bonded oxygen atoms (C=O)~~ and those given by C-O, at 286.0 eV (C-1s) and 532.7 eV (O-1s) [55,56], suggests the presence of these groups at the NP surface. Interestingly, the N-1s peak at 398.2 eV (Figure

2d) broadened after irradiation (Table S1). This indicates the presence of several amine species. The chemical shift of the peak to a lower binding energy (from 400.2 eV to 398.2 eV after synthesis) suggests an interaction of nitrogen-containing functional groups with the NP surface. [52]

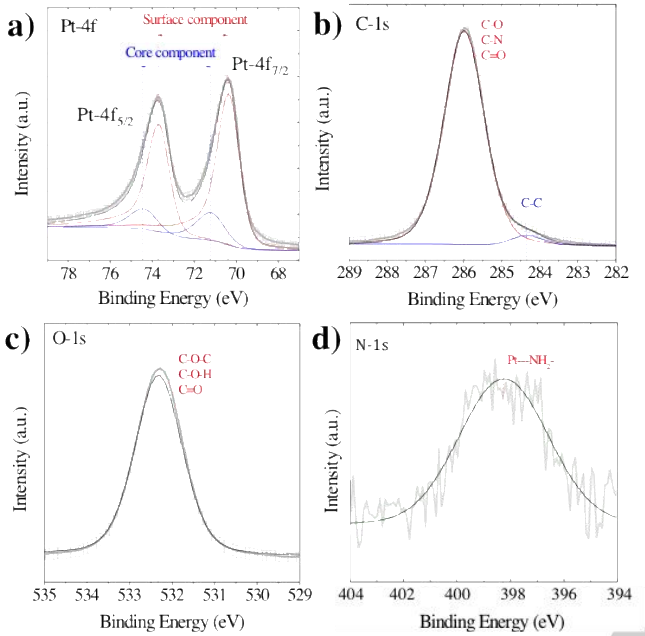

Figure 2. XPS spectra of PtPEG NPs in the ranges of (a) Pt-4f, (b) C-1s, (c) O-1s and (d) N-1s core levels.

The analysis of the surface chemistry was completed using Fourier transform infrared (FT-IR) spectroscopy (Figure 3). The initial compounds and the mixed solution were characterized before and after irradiation. The band located at 3424 cm^{-1} corresponds to the hydroxyl stretching mode ν_{O-H} of the bonded hydrogen of the native PEG-OH [56] (Figure 3a). The peak centred at 2885 cm^{-1} is characteristic of the alkyl stretching mode (ν_{CH_2}) and the peaks in the region from 1000 to 1300 cm^{-1} are characteristic of the stretching vibrational modes of ether (ν_{C-O}). The precursor $Pt(NH_3)_4Cl_2$ (Figure 3b) displayed bands at 3242 and 3135 cm^{-1}, which are attributed to the asymmetric and symmetric vibrational N-H stretching modes (ν_{NH_3}). From 1564 to 842 cm^{-1} the bending and rocking vibrational modes (δ_{HNH} and ρ_{NH_3}) were observed. The IR band at 510 cm^{-1} corresponds to the Pt-N stretching mode. [57]

The interaction of the Pt^{II} precursor with PEG-OH before irradiation was confirmed by FT-IR (Figure 3c). The peaks observed at 3477 and 3286 cm^{-1} are characteristic of the N-H stretching mode (ν_{NH}) of a new amide group. In particular, the IR band at 1642 cm^{-1} is attributed to the C=O stretching vibrational mode of primary amides. This signal overlaps with the 1620 to 1655 cm^{-1} region, which corresponds to the N-H bending vibrational mode of this functional group. At 1453 cm^{-1}, the C-N stretching mode (ν_{CN}) of primary amides was also observed.

vAll these features converge and indicate stable intermediate species are formed before irradiation. The peak at 541 cm^{-1} is attributed to the Pt-N bond and confirms this statement. [58] Its broadening is attributed to the overlap with the C=O bending vibrational mode of amides (535 - 615 cm^{-1} region). We suggest that the $Pt(NH_3)_4Cl_2$ precursor reacts with PEG to form an amide linker due to initial PEG activation. In the presence of oxygen, this activation may take place *via* dehydrogenation (oxidation) of the hydroxyl-end group of the PEG. The oxidation of PEG is thermodynamically favourable. [59] In the present case, the reaction may also be catalysed at room temperature by Pt. [60–62] PEG may be oxidised into aldehydes (-CHO) or carboxylic acids (–COOH), and thus react preferentially with the ammonium ligand ($–NH_3^+$) of the Pt precursor [63] to form a stable conjugation shell (Figure S3). After irradiation, minor changes were observed and the bonds visible by IR remained unchanged (*e.g.* C-O, C=O, O-H and N-H) (Figure 3d). This result suggests that the PEGylation of small Pt NPs is due to Pt-H-N moieties or electrostatic interactions between amide species and Pt, as proposed in other work. [64]

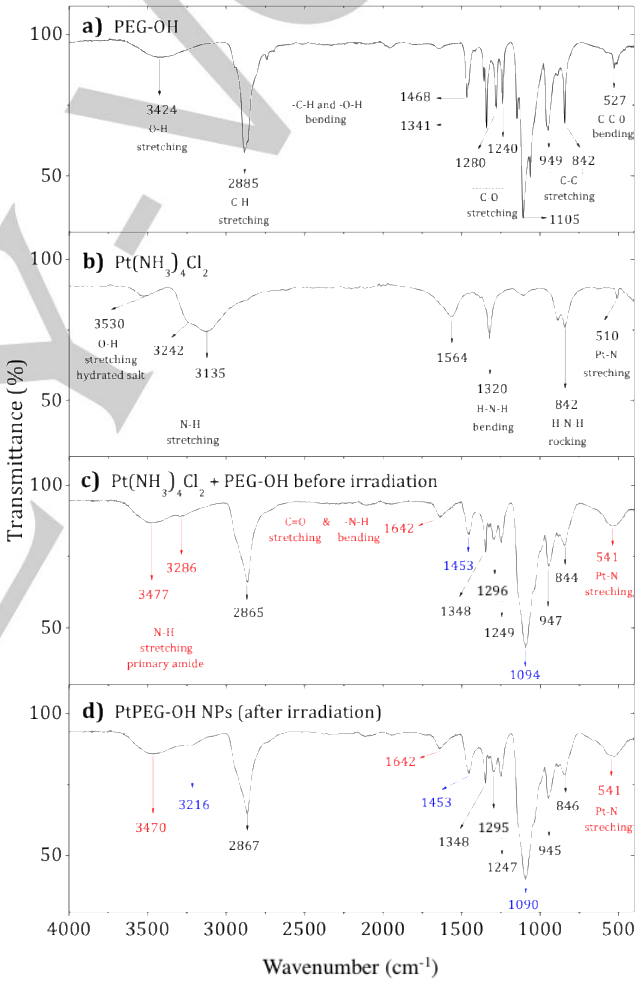

Figure 3. FT-IR spectra of pure PEG-OH (a), pure Pt^{II} precursor (b), Pt^{II} precursor mixed with PEG-OH (before irradiation) (c) and PtPEG NPs obtained after irradiation of the Pt^{II} precursor mixed with PEG-OH (d).

The cytotoxicity of PtPEG NPs in HeLa cells was evaluated by performing colony formation assays (CFA). The plating efficiencies (PE) of the two samples, the control and the cells incubated for 6 hours with PtPEG NPs at a Pt concentration of 5×10^{-4} mol.L^{-1}, were similar (~ 65%, p= 0.42). It indicates that the NPs were not cytotoxic at this concentration. The cytotoxicity

(~30%) appeared at a concentration of 10^{-3} mol.L^{-1} (PE ~ 42%, p= 0.02).

The uptake of PtPEG NPs at a Pt concentration of 5×10^{-4} mol.L^{-1} in HeLa cells was quantified, after 6 hours of incubation, by Inductively Coupled Plasma (ICP) using an Optical Emission Spectrophotometer (OES). The ICP-OES analysis showed that 0.495 Pt µg were internalised by *ca.* 2×10^{6} cells, which corresponds to ~ 5.178×10^{5} NPs per cell. The intracellular mapping of NPs was investigated by means of Nanoscale Secondary Ion Mass Spectrometry (NanoSIMS). The Nano-SIMS analysis was performed on HeLa cells loaded with PtPEG NPs at the non-toxic conditions mentioned before. This technique allows detecting different chemical elements simultaneously (see Figure 4a). The distribution images of phosphorus (P^-) and platinum (Pt^-) are presented in Figure 4b-d (square frame of 50 µm × 50 µm).

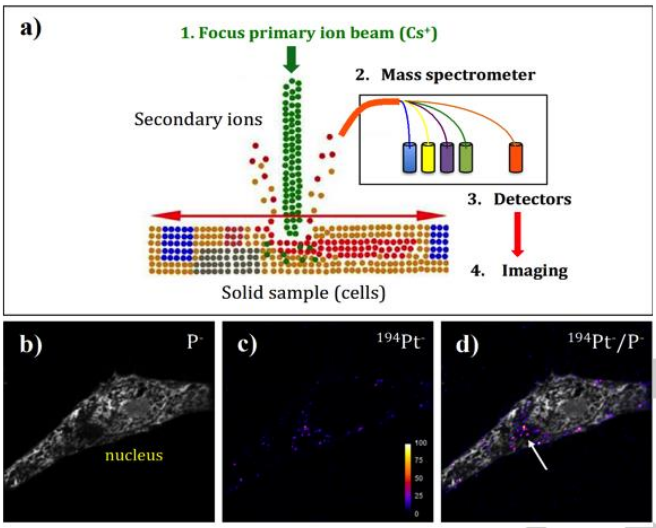

Figure 4. a) Schematic representation of the Nano-SIMS principle (adapted from Jiang fH. *et al* [65]). b-d) Nano-SIMS images of a HeLa cell loaded with PtPEG NPs. The panels b and c correspond to the location of P^- and $^{194}Pt^-$ respectively. The panel d is the merged image of $^{194}Pt^-$ and P^-. The arrow points out the location of NPs in the cell cytoplasm.

The morphological cell structure was derived from the P^- image (Figure 4b). Phosphorus is essentially contained in DNA, RNA and phospholipids. So its detection is used to distinguish individual cells and delineate the nucleus from the cytoplasm. The $^{194}Pt^-$ image (Figure 4c) shows the distribution of Pt compounds. Figure 4d presents the merged image of $^{194}Pt^-$ and P^-. The Nano-SIMS analysis clearly demonstrated the presence of Pt inside the cell. PtPEG NPs were seen in the cytoplasm exclusively but not in the nucleus. This is in agreement with other works performed by the group with Pt complexes [66] and other studies with metal-containing NPs. [67–69] Note that PtPEG NPs preferentially accumulated at cytoplasmic sites poor in phosphorus (region indicated with an arrow). This was observed in other works where 15N-labeled peptide vectors co-localised in HeLa cytoplasmic zones with a low phosphorous concentration. [70]

The impact of PtPEG NPs on cell killing induced by medical carbon ions (provided by the HIMAC hadrontherapy centre, Chiba, Japan) of 290 MeV/u.m.a incident energy and an average linear energy transfer LET of 110 keV.µm^{-1} (5 mm SOBP mode), was evaluated by performing clonogenic assay. For comparison, similar experiments were performed with γ-rays. The survival curves of the controls and cells incubated with PtPEG NPs (Pt 5×10^{-4} mol.L^{-1}, 6 hours) are shown in Figure 5a. The surviving fractions (SF) of cells were determined for doses ranging from 0 up to 5 Gy, and from 0 up to 2.5 Gy for γ-rays and carbon ions, respectively.

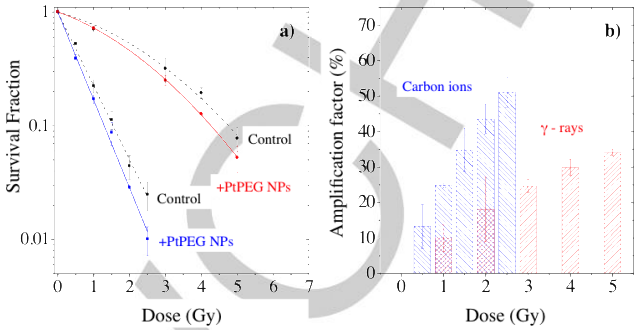

Figure 5. (a) Surviving fractions of HeLa cells irradiated by γ-rays (●, ●) and carbon ions (■, ■) in controls and in the presence of PtPEG NPs as a function of the radiation dose. (b) Amplification factors as a function of the radiation doses for γ-rays (red columns) and carbon ion beams (blue columns).

The cell response curves were simulated using the linear quadratic (LQ) model:

$$SF(D) = e^{-(\alpha D+\beta D^2)} \quad (5)$$

where the parameter α is attributed to the induction of directly lethal damage and β to the additive sub-lethal lesions leading to cell death. [71,72] The analysis shows that PtPEG NPs induced an increase of α from 0.15 to 0.26 with γ-rays and from 1.50 to 1.78 with carbon ion radiation. Contrary β remained nearly constant. So, the presence of PtPEG NPs during carbon irradiation enhances cell killing as due to the increasing induction of directly lethal damages (α).

The efficiency of PtPEG NPs to amplify cancer cell killing was quantified using the amplification factor (AF), and the dose-enhancing factor (DEF).

AF was used to quantify the efficiency of NPs to enhance cell killing at a defined dose point (D). It is equivalent to the radiation sensitising enhancement ratio (SER) commonly used to describe cell-specific radiosensitisation effects. [68] AF was calculated as follows:

$$AF = \frac{SF_{control}^{fitted\ curve} - SF_{PtPEG\ NPs}^{fitted\ curve}}{SF_{control}^{fitted\ curve}} \times 100\ [=]\ \% \quad (6)$$

$SF_{control}^{fitted\ curve}$ and $SF_{PtPEG\ NPs}^{fitted\ curve}$ correspond, respectively, to the survival fraction of the control and the survival fraction of the cells loaded with NPs, obtained at the same irradiation dose. The values are reported in Figure 5b. Interestingly, at 2 Gy, the AF increased by 44% with incident carbon ions and 14% with γ-rays. This clearly shows that the amplification of cell killing with carbon ions is stronger than with γ-rays at the same dose.

DEF is commonly used to assess the dose enhancement *in vitro* for a given survival fraction, commonly 10% of survival (SF = 10%). [73]

$$DEF = \frac{D^{10}control}{D^{10}\ PtPEG\ NPs} \quad (7)$$

where D^{10} corresponds to the dose required to reach 10% survival. DEFs of 1.1 and 1.19 were found for γ-rays and carbon ion irradiations, respectively. This corresponds to dose enhancements of about 10% and 16%, respectively, confirming that PtPEG NPs are more efficient for improving the lethality of carbon ions than γ-rays. It indicates that lower radiation doses are needed to obtain the same effect, in particular for carbon ions.

We evaluated the relative biological efficiency (RBE) at 10% of survival using γ-rays as a reference beam. [74]

$$\mathrm{RBE}_{\mathrm{control}} = \frac{\mathrm{D}^{10}_{\gamma\mathrm{rays\ control}}}{\mathrm{D}^{10}_{\mathrm{C}^{6+}\ \mathrm{control}}} \quad (8)$$

and

$$\mathrm{RBE}_{\mathrm{NPs}} = \frac{\mathrm{D}^{10}_{\gamma\ \mathrm{rays\ control}}}{\mathrm{D}^{10}_{\mathrm{C}^{6+}\ \mathrm{with\ NPs}}} \quad (9)$$

The RBE was found close to 3.09 for free HeLa cells, which is in good agreement with other works. [16] In the presence of PtPEG NPs, the RBE value was 3.68 which is a ~19% increase. This result clearly demonstrates that the treatment of HeLa cells with PtPEG NPs increased the RBE of carbon ions.

The interaction of ionising radiation with biomolecules leads to bond cleavages in nucleic acids, lipids and proteins. It is commonly accepted that complex damage of sizes in the nanometer range are the most lethal for cells. In order to characterise the impact of NPs on the induction of complex lesions, we used DNA plasmids as bio-nanoprobes and quantified the induction of double strand breaks (DSB). The average number of nanosize damage per plasmid induced in the bio-nanoprobes free of NPs (control) and in the presence of PtPEG NPs at different radiation doses, is presented in Figure 6. In some experiments, dimethyl sulfoxide (DMSO), a well-known radical scavenger with redox potential 0.16 V, was added to disentangle the effect of water radicals, in particular the highly reactive hydroxyl radicals ($OH^{\cdot}$). [75]

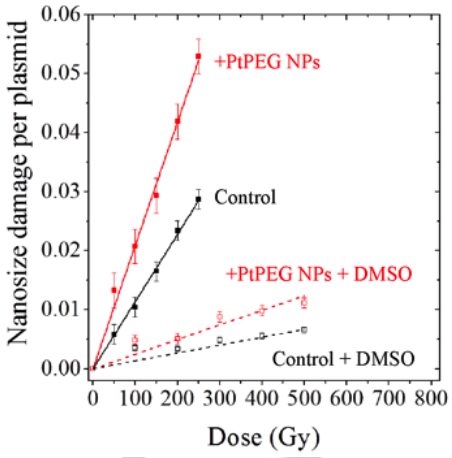

Figure 6. Nanosize damage induced by γ-rays in bio-probes free of NPs (■) and in the presence of PtPEG NPs (■), as a function of the irradiation dose. Results obtained in the presence of DMSO in bio-probes free of NPs (□) or with PtPEG-OH NPs (□).

The induction of nanosize damage increased linearly with the irradiation dose for all the samples. It indicates that damages were induced by single ionising events. [76] In the presence of PtPEG NPs, the induction of nanosize damage was strongly amplified. It sharply decreased in the presence of DMSO (dotted lines). This is in agreement with previous studies performed with metal-based NPs activated by photons [23,75] or by incident ions. [24–26]

The yields of nanosize damage in NPs free samples ($\mathrm{yield}_{\mathrm{control}}$) and NPs loaded samples ($\mathrm{yield}_{\mathrm{PtPEG\ NPs}}$) correspond to the slopes of the respective dose response curves. The values are reported in **Table 2.** The efficiency of PtPEG NPs to amplify the induction of nanosize damage was quantified using the molecular amplification factor (mAF):

$$\mathrm{mAF} = \frac{\mathrm{yield}_{\mathrm{PtPEG\ NPs}} - \mathrm{yield}_{\mathrm{control}}}{\mathrm{yield}_{\mathrm{control}}} \times 100 \quad (10)$$

In the presence of PtPEG NPs, the induction of nanosize damage was enhanced by a factor of 83% (from 11.40×10^{-5} to 20.90×10^{-5} damage per plasmid per Gy). On the other hand, the presence of DMSO decreased the yield of nanosize damage (from 20.90×10^{-5} to 2.48×10^{-5}), which indicates that the amplification of complex damage by PtPEG NPs, was mediated by water radicals by ~ 90%.

Table 2. Yields of controls and plasmids loaded with PtPEG NPs with a NP:plasmid ratio close 4:1. DMSO was added in some experiments. The mAF is also reported.

Sample	Nanosize breaks/plasmid/Gy $\times10^{-5}$	mAF (%)	OH effect (%)
Control	11.40 ± 0.25	-	-
+ PtPEG NPs	20.90 ± 0.21	83 ± 4	-
Control + DMSO	1.34 ± 0.18	-	88 ± 1
+ PtPEG NPs + DMSO	2.48 ± 0.11	85 ± 15	88 ± 1

In summary, the amplification of complex damage by Pt NPs is attributed to a sequence of physical and chemical processes. [12,25] Briefly, Pt NPs are activated (ionised) by the incident radiation (*e.g.* photons or particles) and related secondary electrons produced along the track. The probability of ionisation and consecutively the number of electrons emitted locally increases with the atomic number (Z) of the compounds in the NPs. In addition, relaxation processes such as Auger de-excitation, [77] plasmon de-excitation [78] and electron capture [79,80] take part in the emission of electrons. The excitation and ionisation of water molecules close to the NPs lead to the production of highly reactive (radicals) nano-clusters. The interaction of these radical clusters with biomolecules will cause nanosize lesions. The activation of PtPEG NPs and the induction of spatially confined perturbations are toxic for cells.

Conclusion

This work presents a simple, fast, scalable and eco-freendly method to produce non-toxic metallic nanoagents dispersed in sterile water solution with a remarkable production rate of 100%, ready-to-use in clinic. As a first example, the synthesis of small

negatively charged PEGylated Pt NPs is presented. The method consists of a one-step radiolytic protocol combined with *in situ* PEGylation.

As a major characteristic, the PEGylated Pt NPs have the singular property to improve the performance of medical radiations, particularly the effect of hadrontherapy beams as shown by the 44% amplification of cell killing induced by carbon ions. The enhancement of complex biodamage confirms that the amplification of radiation effects is due to a cascade of early stage mechanisms that follow the activation of nanoparticles by radiation. This finding is important to improve the composition of future nanoagents and simulate treatment planning.

Radiolysis is currently used in large scale by private stakeholders to decontaminate food or sterilise medical material. Therefore, the production of non-toxic metallic nanoagents using this singular method may be transposable to industrial production in the medium term.

Dense metallic materials are well detected in computed tomography (CT). Moreover PEGylated Pt NPs may be functionalized with elements active in Positron-emission tomography (PET) or Magnetic resonance imaging (MRI) @(*e.g.* ^{89}Zr for PET, Gd for MRI). Thus, the remarkable competitiveness of this synthesis reinforces the development of advanced radiation strategies such as "image guided radiation therapy".

Acknowledgements

The authors acknowledge the Mexican National Council for Science and Technology (CONACyT) for supporting D. Salado-Leza through a PhD CONACyT – Gobierno Francés scholarship (216823 / 312283), the China Scholarship Council for granting X. Yang (CSC, N° 201607040068), the European Commission for the two grants PEOPLE-ITN-ARGENT no. 608163 and PEOPLE-IEF-NANOHAPY no. 624370, the Japanese Society for the Promotion of Sciences (JSPS) for a visiting grant offered to M. Bolsa. A part of this research was conducted as research project at NIRS-HIMAC. HR-TEM measurements were performed with the collaboration of P. Beaunier (Laboratoire de Réactivité des Surfaces, Sorbonne Université). The French team acknowledges E. Sage (Institut Curie, Orsay, France) for her strong support in the first cell experiments.

Keywords: Platinum nanoparticles • Radiotherapy • Hadron therapy • Radiolytic synthesis• Green synthesis

[1] K. Kobayashi, H. Frohlich, N. Usami, K. Takakura, C. Le Sech, *Radiat. Res.* **2002**, *157*, 32–7.

[2] M.-C. Biston, A. Joubert, J.-F. Adam, H. Elleaume, S. Bohic, A. Charvet, F. Estève, N. Foray, J. Balosso, *Cancer Res.* **2004**, *64*, 2317–2323.

[3] J. F. Hainfeld, D. N. Slatkin, H. M. Smilowitz, *Phys. Med. Biol.* **2004**, *49*, N309–N315.

[4] J. F. Hainfeld, F. A. Dilmanian, D. N. Slatkin, H. M. Smilowitz, *J Pharm Pharmacol* **2008**, *60*, 977–85.

[5] Y. Li, K. H. Yun, H. Lee, S. H. Goh, Y. G. Suh, Y. Choi, *Biomaterials* **2019**, *197*, 12–19.

[6] S. Bonvalot, C. Le Pechoux, T. De Baere, G. Kantor, X. Buy, E. Stoeckle, P. Terrier, P. Sargos, J. M. Coindre, N. Lassau, et al., *Clin. Cancer Res.* **2017**, *23*, 908–917.

[7] F. Lux, V. L. Tran, E. Thomas, S. Dufort, F. Rossetti, M. Martini, C. Truillet, T. Doussineau, G. Bort, F. Denat, et al., *Br. J. Radiol.* **2019**, *92*, 1–19.

[8] C. Verry, L. Sancey, S. Dufort, G. Le Duc, C. Mendoza, F. Lux, S. Grand, J. Arnaud, J. Louis Quesada, J. Villa, et al., *BMJ Open* **2019**, *9*, DOI 10.1136/bmjopen-2018-023591.

[9] S. K. Libutti, G. F. Paciotti, A. A. Byrnes, H. R. Alexander, W. E. Gannon, M. Walker, G. D. Seidel, N. Yuldasheva, L. Tamarkin, *Clin. Cancer Res.* **2010**, *16*, 6139–6149.

[10] E. Porcel, K. Kobayashi, N. Usami, H. Remita, C. Le Sech, S. Lacombe, *J. Phys. Conf. Ser.* **2011**, *261*, 012004.

[11] K. T. Butterworth, S. J. McMahon, F. J. Currell, K. M. Prise, *Nanoscale* **2012**, *4*, 4830.

[12] Y. Wang, J. Liu, X. Ma, X. J. Liang, *Nano Res.* **2018**, *11*, 2932–2950.

[13] M. Durante, J. S. Loeffler, *Nat. Rev. Clin. Oncol.* **2010**, *7*, 37–43.

[14] V. Vitolo, M. R. Fiore, A. Barcellini, B. Vischioni, A. Iannalfi, A. Facoetti, P. Fossati, M. Bonora, S. Ronchi, E. D'Ippolito, et al., *Anticancer Res.* **2019**, *39*, 909–913.

[15] IAEA and ICRU, **2008**, *461*.

[16] H. Kaur, G. Pujari, M. K. Semwal, A. Sarma, D. K. Avasthi, *Nucl. Instruments Methods Phys. Res. Sect. B Beam Interact. with Mater. Atoms* **2013**, *301*, 7–11.

[17] J.-K. Kim, S.-J. Seo, K.-H. Kim, T.-J. Kim, M.-H. Chung, K.-R. Kim, T.-K. Yang, *Nanotechnology* **2010**, *21*, 425102.

[18] G. Dollinger, *Nanotechnology* **2011**, *22*, 248001.

[19] C. Le Sech, K. Kobayashi, N. Usami, Y. Furusawa, E. Porcel, S. Lacombe, *Appl. Phys. Lett.* **2012**, *100*, 026101.

[20] F. Li, Z. Li, X. Jin, Y. Liu, P. Li, Z. Shen, A. Wu, X. Zheng, W. Chen, Q. Li, *Nanoscale Res. Lett.* **2019**, *14*, DOI 10.1186/s11671-019-3152-2.

[21] R. Abdul Rashid, S. Zainal Abidin, M. A. Khairil Anuar, T. Tominaga, H. Akasaka, R. Sasaki, K. Kie, K. Abdul Razak, B. T. T. Pham, B. S. Hawkett, et al., *OpenNano* **2019**, *4*, 100027.

[22] S. Li, S. Bouchy, S. Penninckx, R. Marega, O. Fichera, B. Gallez, O. Feron, P. Martinive, A.-C. Heuskin, C. Michiels, et al., *Nanomedicine* **2019**, *14*, 317–333.

[23] D. Salado-Leza, A. Traore, E. Porcel, D. Dragoe, A. Muñoz, H. Remita, G. García, S. Lacombe, *Int. J. Mol. Sci.* **2019**, *20*, 5648.

[24] T. Schlatholter, P. Eustache, E. Porcel, D. Salado, L. Stefancikova, O. Tillement, F. Lux, P. Mowat, M.-J. van Goethem, H. Remita, et al., *Int. J. Nanomedicine* **2016**, *11*, 1549.

[25] E. Porcel, S. Liehn, H. Remita, N. Usami, K. Kobayashi, Y. Furusawa, C. Le Sech, S. Lacombe, *Nanotechnology* **2010**, *21*, 85103.

[26] E. Porcel, O. Tillement, F. Lux, P. Mowat, N. Usami, K. Kobayashi, Y. Furusawa, C. Le Sech, S. Li, S. Lacombe, *Nanomedicine* **2014**, *10*, 1601–1608.

[27] C. Alric, I. Miladi, D. Kryza, J. Taleb, F. Lux, R. Bazzi, C. Billotey, M. Janier, P. Perriat, S. Roux, et al., *Nanoscale* **2013**, *5*, 5930–9.

[28] L. Maggiorella, G. Barouch, C. Devaux, A. Pottier, E. Deutsch, J. Bourhis, E. Borghi, L. Levy, *Futur. Oncol.* **2012**, *8*, 1167–1181.

[29] A. Mignot, C. Truillet, F. Lux, L. Sancey, C. Louis, F. Denat, F. Boschetti, L. Bocher, A. Gloter, O. Stéphan, et al., *Chem. - A Eur. J.* **2013**, *19*, 6122–6136.

[30] D. Pedone, M. Moglianetti, E. De Luca, G. Bardi, P. P. Pompa, *Chem. Soc. Rev* **2017**, *46*, 4951–4975.

[31] A. Abedini, A. R. Daud, M. A. Abdul Hamid, N. Kamil Othman, E. Saion, *Nanoscale Res. Lett.* **2013**, *8*, 474.

[32] B. Akar, K. Pushpavanam, E. Narayanan, K. Rege, J. J. Heys, *Biomed. Phys. Eng. Express* **2018**, *4*, 549–59.

[33] A. M. Abdelghany, E. M. Abdelrazek, S. I. Badr, M. S. Abdel-Aziz, M. A. Morsi, *J. Saudi Chem. Soc.* **2017**, *21*, 528–537.

[34] J. Biswal, S. P. Ramnani, S. Shirolikar, S. Sabharwal, *Int. J. Nanotechnol.* **2010**, *7*, 907–918.

[35] T. K. L. Nguyen, N. D. Nguyen, V. P. Dang, D. T. Phan, T. H. Tran, Q. H. Nguyen, H. D. Mai, *Adv. Mater. Sci. Eng.* **2019**, *2019*, 1–6.

[36] T. Cele, M. Maaza, A. Gibaud, *MRS Adv.* **2018**, *3*, 2537–2557.

[37] B. Keita, L. Nadjo, C. De Cointet, J. Amblard, J. Belloni, *Chem. Phys. Lett.* **1996**, *249*, 297–303.

[38] E. Gharibshahi, E. Saion, A. Ashraf, L. Gharibshahi, *Appl. Radiat. Isot.* **2017**, *130*, 211–217.

[39] A. D. Belapurkar, S. Kapoor, S. K. Kulshreshtha, J. P. Mittal, *Mater. Res. Bull.* **2001**, *36*, 145–151.

[40] W. Pasanphan, L. Chunkoh, S. Choofong, *ICCM Int. Conf. Compos. Mater.* **2011**, 6–11.

[41] M. Treguer, C. de Cointet, H. Remita, J. Khatouri, M. Mostafavi, J. Amblard, J. Belloni, R. de Keyzer, *J. Phys. Chem. B* **1998**, *102*, 4310–4321.

[42] H. Remita, I. Lampre, M. Mostafavi, E. Balanzat, S. Bouffard, *Radiat. Phys. Chem.* **2005**, *72*, 575–586.

[43] H. Remita, S. Remita, in *Recent Trends Radiat. Chem.* (Eds.: J.F. Wishart, B.S. Madhava Rao), World Scientific, **2010**, pp. 347–383.

[44] E. Gharibshahi, E. Saion, *Int. J. Mol. Sci.* **2012**, *13*, 14723–14741.

[45] K. Huang, H. Ma, J. Liu, S. Huo, A. Kumar, T. Wei, X. Zhang, S. Jin, Y. Gan, P. C. Wang, et al., *ACS Nano* **2012**, *6*, 4483–4493.

[46] C. Puglia, A. Nilsson, B. Hernnäs, O. Karis, P. Bennich, N. Mårtensson, *Surf. Sci.* **1995**, *342*, 119–133.

[47] F. Liu, Z. Zhao, L. Qiu, L. Zhao, *J. Surf. Anal.* **2009**, *15*, 271–273.

[48] X. Fu, Y. Wang, N. Wu, L. Gui, Y. Tang, *J. Colloid Interface Sci.* **2001**, *243*, 326–330.

[49] G. P. López, D. G. Castner, B. D. Ratner, *Surf. Interface Anal.* **1991**, *17*, 267–272.

[50] L. M. Forbes, A. M. O'Mahony, S. Sattayasamitsathit, J. Wang, J. N. Cha, *J. Mater. Chem.* **2011**, *21*, 15788.

[51] L. M. Forbes, S. Sattayasamitsathit, P. F. Xu, A. O'Mahony, I. A. Samek, K. Kaufmann, J. Wang, J. N. Cha, *J. Mater. Chem. A* **2013**, *1*, 10267–10273.

[52] X. Crispin, R. Lazzaroni, A. Crispin, V. . Geskin, J. . Brédas, W. . Salaneck, *J. Electron Spectros. Relat. Phenomena* **2001**, *121*, 57–74.

[53] R. J. J. Jansen, H. van Bekkum, *Carbon N. Y.* **1995**, *33*, 1021–1027.

[54] G. Deniau, L. Azoulay, P. Jégou, G. Le Chevallier, S. Palacin, *Surf. Sci.* **2006**, *600*, 675–684.

[55] C. M. Whelan, J. Ghijsen, J.-J. Pireaux, K. Maex, *Thin Solid Films* **2004**, *464*, 388–392.

[56] R. M. Silverstein, G. C. Bassler, T. C. Morrill, *Spectrometric Identification of Organic Compounds*, Wiley, **1991**.

[57] K. Nakamoto, *Infrared and Raman Spectra of Inorganic and Coordination Compounds. Part B: Applications in Coordination, Organometallic and Bioinorganic Chemistry*, John Wiley & Sons. Inc., Hoboken, New Jersey, **2009**.

[58] R. Wysokiski, J. Kuduk-Jaworska, D. Michalska, *J. Mol. Struct. THEOCHEM* **2006**, *758*, 169–179.

[59] J. Glastrup, *Polym. Degrad. Stab.* **1996**, *52*, 217–222.

[60] S. Chibani, C. Michel, F. Delbecq, C. Pinel, M. Besson, *Catal. Sci. Technol.* **2013**, *3*, 339–350.

[61] T. Mallat, A. Baiker, *Catal. Today* **1994**, *19*, 247–283.

[62] R. Anderson, K. Griffin, P. Johnston, P. L. Alsters, *Adv. Synth. Catal.* **2003**, *345*, 517–523.

[63] S. Cox Gad, *Handbook of Pharmaceutical Biotechnology*, John Wiley & Sons. Inc., **2007**.

[64] P. Wand, J. D. Bartl, U. Heiz, M. Tschurl, M. Cokoja, *J. Colloid Interface Sci.* **2016**, *478*, 72–80.

[65] H. Jiang, C. N. Goulbourne, A. Tatar, K. Turlo, D. Wu, A. P. Beigneux, C. R. M. Grovenor, L. G. Fong, S. G. Young, *J. Lipid Res.* **2014**, *55*, 2156–66.

[66] N. Usami, Y. Furusawa, K. Kobayashi, S. Lacombe, A. Reynaud-Angelin, E. Sage, T. Di Wu, A. Croisy, J. L. Guerquin-Kern, C. Le Sech, *Int. J. Radiat. Biol.* **2008**, *84*, 603–611.

[67] L. Stefančíková, E. Porcel, P. Eustache, S. Li, D. Salado, S. Marco, J.-L. Guerquin-Kern, M. Réfrégiers, O. Tillement, F. Lux, et al., *Cancer Nanotechnol.* **2014**, *5*, 6.

[68] S. Jain, J. A. Coulter, A. R. Hounsell, K. T. Butterworth, S. J. McMahon, W. B. Hyland, M. F. Muir, G. R. Dickson, K. M. Prise, F. J. Currell, et al., *Int. J. Radiat. Oncol. Biol. Phys.* **2011**, *79*, 531–9.

[69] N. B. Shah, J. Dong, J. C. Bischof, *Mol. Pharm.* **2011**, *8*, 176–184.

[70] W. Romer, T.-D. Wu, P. Duchambon, M. Amessou, D. Carrez, L. Johannes, J.-L. Guerquin-Kern, *Appl. Surf. Sci.* **2006**, *252*, 6925–6930.

[71] M. Tubiana, J. Dutreix, A. Wambersie, in *Radiobiologie*, Hermann, Éditeurs Des Sciences Et Des Arts, Paris, **1986**, pp. 73–104.

[72] B. G. Douglas, J. F. Fowler, *Radiat. Res.* **1976**, *66*, 401–426.

[73] L. E. Taggart, S. J. McMahon, F. J. Currell, K. M. Prise, K. T. Butterworth, *Cancer Nanotechnol.* **2014**, *5*, 5.

[74] International Commission on Radiological Protection, *Health Phys.* **1963**, *9*, 357–386.

[75] E. Porcel, S. Li, N. Usami, H. Remita, Y. Furusawa, K. Kobayashi, C. Le Sech, S. Lacombe, *J. Phys. Conf. Ser.* **2012**, *373*, 012006.

[76] M. A. Śmiałek, S. A. Moore, N. J. Mason, D. E. G. Shuker, *Radiat. Res.* **2009**, *172*, 529–536.

[77] S. J. McMahon, W. B. Hyland, M. F. Muir, J. A. Coulter, S. Jain, K. T. Butterworth, G. Schettino, G. R. Dickson, A. R. Hounsell, J. M. O'Sullivan, et al., *Radiother. Oncol.* **2011**, *100*, 412–416.

[78] A. V. Verkhovtsev, A. V. Korol, A. V. Solov'yov, *J. Phys. Chem. C* **2015**, *119*, 11000–11013.

[79] Z. D. Pešić, R. Hellhammer, B. Sulik, N. Stolterfoht, *J. Phys. B At. Mol. Opt. Phys.* **2009**, *42*, 235202.

[80] H. Stumpf, *Phys. der Kondens. Mater.* **1971**, *13*, 101–117.

Entry for the Table of Contents

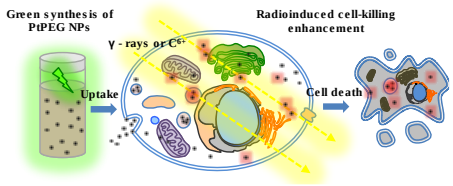

A simple and green strategy to synthesize small, non-toxic and stable metallic nanoparticles with a 100% production rate. Platinum nanoparticles coated with biocompatible ligands are presented as proof of concept. They are internalized by cancerous cells and amplify the cell killing induced by γ-rays and carbon ions used in hadrontherapy, triggering nanosize molecular breaks. This method opens a new era for NPs-aided radiation therapies.